Investigating the Effect of Annealing Temperature on Structural, Luminescence, and Magnetic Properties of Nickel and Zinc Aluminate

Sampurnanand, Nishant Kumar, Rakesh Kumar Singh, Atul Jyoti, and Vikash Kumar

1 Introduction

Spinal structured aluminate is a compound containing aluminum and oxygen with more electropositive elements that is a salt of the hypothetical aluminic acid. It is broadly used in water purification, manufacture of zeolites, ceramics, petrochemical industry, and photocatalysts due to its thermal resistance, electronics, and optical properties [1–6]. Generally, the spinal structure is formulated as $A^{2+}B_2{}^{3+}O_4$ in which A and B are known as divalent and trivalent metal ions. Spinal structure may be classified as A^{2+} occupy eight tetrahedral holes, B^{3+} occupy four octahedral holes, and the anions are arranged in a cubic close packed lattice which belongs to fd-3 m space group [7–9]. Zinc aluminates ($ZnAl_2O_4$) are well-known luminescent materials emitting in the visible region when doped with suitable activators such as rare earth and transition metal ions [10, 11]. Zinc aluminates have high thermal stability, high mechanical resistance, hydrophobicity, and magnificent optical properties; due to this ability, they may be used as a ceramic, electro-conductive material, and catalyst [5, 12]. Nickel aluminate ($NiAl_2O_4$) has received attention as a catalyst solid support due to its stability, strong resistance to acids and alkalis, and high melting point [13]. Nickel aluminates are one of the most important aluminates materials used in many applications such as magnetic materials, catalysts, pigments, sensors, and refractory materials [14–17]. Spinal metal aluminates can be synthesized by various methods such as co-precipitation, combustion, hydrothermal, micro-emulsions, electrodeposition, solid-state reactions, and sol–gel methods [18–22]. Generally, nanosized metal aluminates are synthesized by solid-state

Sampurnanand · N. Kumar · R. K. Singh (✉) · A. Jyoti
School of Engineering and Technology, Aryabhatta Centre for NanoScience and Nanotechnology, Aryabhatta Knowledge University, Patna 800001, India

V. Kumar
Department of Mechanical Engineering, Maulana Azad National Institute of Technology (MANIT), Bhopal, India

P. Verma et al. (eds.), *Advancement in Materials, Manufacturing and Energy Engineering, Vol. I*, Lecture Notes in Mechanical Engineering,
https://doi.org/10.1007/978-981-16-5371-1_32

reaction, but the main disadvantage of this method is using a high temperature of more than 1000 °C [23, 24]. Due to this high temperature, product is obtained with low surface area, heterogeneous, and lack of morphology control [25]. The sol–gel approach is an effective and low temperature technique that allows the stoichiometric control of the products chemical composition and produces homogeneous materials [26]. Sol–gel is a facile way to synthesize nanoparticles from aqueous salt solution by the addition of a base under inert atmosphere at room temperature or at elevated temperature [27]. The significance of the sol–gel process as compared to other methods is that it includes the ability to maintain a high degree of purity, high homogeneity, and high surface area at low temperature [28].

In the present work, pure phase nickel and zinc aluminate material has been synthesized using sol–gel method and effect of annealing on structural parameters like (crystallite size, lattice strain etc.) luminescence and magnetic properties. To the best of my knowledge very few research finding are available on optical properties of aluminate and its annealing effect.

2 Experimental

2.1 Materials

All the compositions of $NiAl_2O_4$ and $ZnAl_2O_4$ nanoparticles were prepared from Merck Germany GR grade chemicals viz $Ni(NO_3)_2.6H_2O$, $Zn(NO_3)_2.6H_2O$, $Al(NO_3)_3.9H_2O$, and aqueous NH_3 (Merck India, 30%). The chemicals obtained were used as received without any further purification.

2.2 Synthesis of $NiAl_2O_4$ and $ZnAl_2O_4$ Nanoparticles

2.2.1 Synthesis of $NiAl_2O_4$ Nanoparticles

In the present study, Ni aluminate nanoparticles have been synthesized using suitable precursors by the sol–gel method. Nickel nitrate, (99% assay), aluminum nitrate (99.9% assay), and citric acid (99% assay) as a chelating agent were used for synthesis of $NiAl_2O_4$ nanoparticles. Schematic diagram of preparation method of nickel aluminate is shown in Fig. 1a. Nickel nitrate (290.79 gm/mole), aluminum nitrate (750.26 gm/mole), and citric acid (768.48 gm/mole) were taken after weighing. Firstly, nickel nitrate is mixed in deionized water which is 20 ml, and then, aluminum nitrate in another beaker separately mixed with deionized water. All three chemicals are mixed in one beaker and shifting of pH with the help of ammonia (NH_3) at pH 7. Then, it was put on magnetic stirrer for 4–5 h at 80 rpm for preparing a homogenous mixture. The solution obtained was then evaporated at

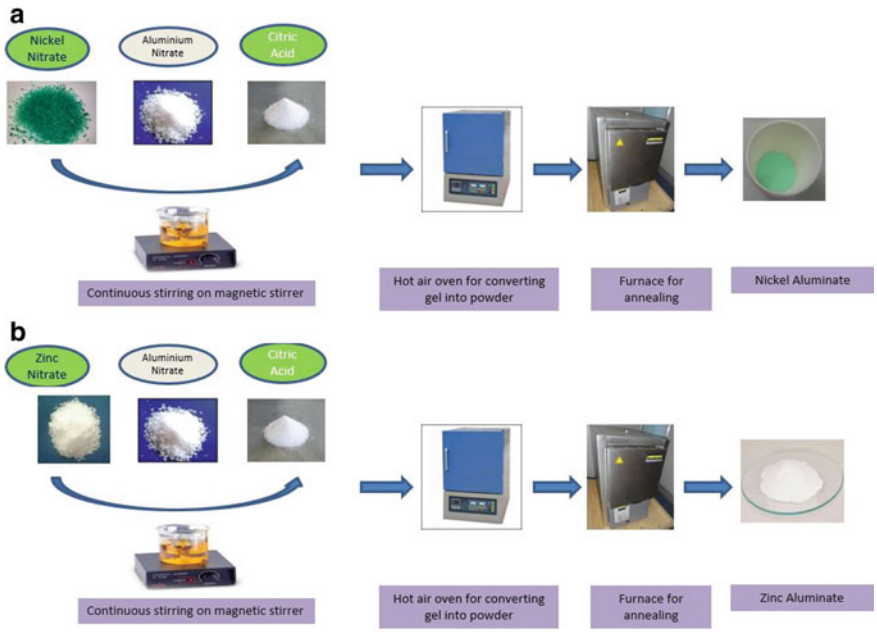

Fig. 1 **a** Schematic diagram of nickel aluminate. **b** Schematic diagram of zinc aluminate

80 °C to get a gel. Then, gel was dried in an oven and obtained nickel aluminate powder. Finally, nickel aluminate was annealed at 650, 750, and 850 °C for 2 h in muffle furnace (Nabertherm, Germany).

2.2.2 Synthesis of $ZnAl_2O_4$ Nanoparticles

In case of Zinc aluminate, zinc nitrate (99.9% assay) 297.47 mol/gm, aluminum nitrate (99.9% assay) 750.26 mol/gm, and citric acid (99% assay) 768.48 gm/mole were used for synthesis. Schematic diagram of synthesis method of zinc aluminate is shown in Fig. 1b. Zinc nitrate is mixed in 20 ml deionized water in a beaker, and aluminum nitrate is mixed with 20 ml deionized water in another beaker. All three chemicals are mixed and shift the pH value with the help of ammonia (NH_3) at pH 7. Afterword similar process was used as used in synthesis of nickel aluminate. The precise measurement of the properties of the synthesized material has the upmost importance in the field of research. In the present study, the synthesized samples were characterized by modern sophisticated instruments namely XRD, VSM, and PL in order to reveal the physical properties.

3 Results and Discussion

3.1 X-Ray Diffraction Measurement

X-ray diffraction pattern of powder $ZnAl_2O_4$ has been obtained using a Bruker D8 X-ray diffractometer as shown in Fig. 2a. The crystallite size of the prepared $ZnAl_2O_4$ particles was calculated applying Scherer's Eq. (1), particularly to the peak having highest intense value at angular location $2\Theta = 36.75°$ (Fig. 2a). Powder X-ray diffraction graph reveals that all samples were of single phase cubic in nature possessing spinel structure [29]. The crystalline size calculated using Scherer's equation given below [30].

$$d = \frac{0.9\lambda}{B \cdot \mathrm{Cos}\theta} \tag{1}$$

In which d represents the average crystallite size, λ is the wavelength of X-ray, B is the peak width at half-maximum height, 0.9 is known as shape factor, and θ is for Bragg's incident angle. The crystalline size obtained was 18 nm, 28 nm, and 30 nm for annealing temperatures of 650 °C, 750 °C, and 850 °C, respectively. It concludes that crystallinity size of $ZnAl_2O_4$ particles increases with annealing temperature. All the diffraction peaks were found to be perfectly at 2θ positions (31.2°), (36.75°), (44.7°), (59.3°), and (65.3°) which signifies to (220), (311), (400), (511), and (440) crystallographic planes, respectively, which are in agreement with the reported values. This indicates that the complete formation of $ZnAl_2O_4$ spinel phase with reference that zinc aluminate is a cubic crystal system spinel structure (JCPDS file no. 98–007-5098) of Fd3m space group. Moreover, absence of any extra peaks reveals impurities which were negligible in the synthesized sample.

For the same three different annealing temperatures of 650, 750, and 850 °C, XRD patterns of nickel aluminate are shown in Fig. 2b. The sample consisted of moderate crystalline $NiAl_2O_4$ particles being present as a single phase. But degree of crystallinity is quite different from that of zinc aluminate. Although both the materials were prepared with same thermodynamic parameters and utilizing same chemical based citrate precursor method, result shows that nucleation and growth mechanism of both Zn aluminate and Ni aluminate crystal is different. The thermal analysis measurement is required for better understanding of thermal decomposition. This is our future work. Further, the XRD spectrum contains desirable five signature peaks in coincidence with the standard data of the cubic spinel Ni aluminate phase (JCPDS card No. 98–007-2075). The peaks of the prepared solid powders were referred to the crystal plane of spinel nickel aluminate, which planes having miller indices {220}, {311}, {400}, {511}, and {440} as shown in Fig. 2b. The nickel aluminate crystals possess spinel form and have got space group Fd3m. Average crystallite size was calculated using Scherer's formula and was found to be 8 nm, 12 nm, and 14 nm, respectively. The lattice parameter (a) is calculated from the peak with highest intensity {311} using the following equation [30]

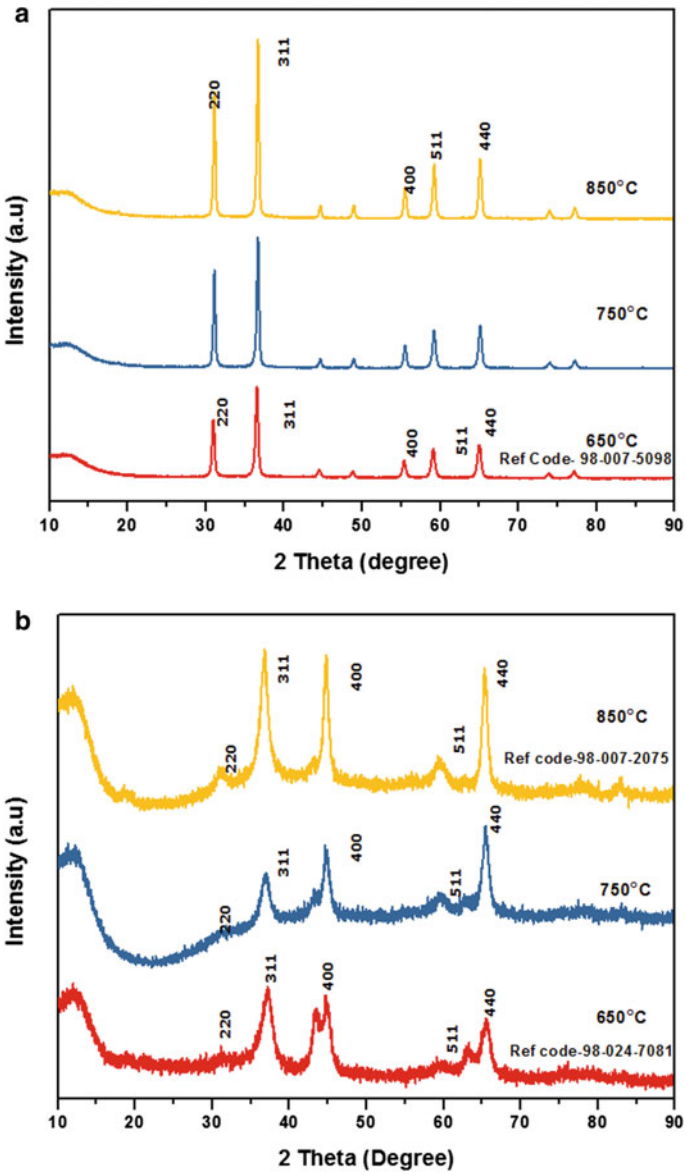

Fig. 2 **a** XRD spectra of $ZnAl_2O_4$ at various annealing temperatures. **b** XRD spectra of $NiAl_2O_4$ at various annealing temperatures

Table 1 (a-b) Lattice parameters for $ZnAl_2O_4$ and $NiAl_2O_4$

Nickel aluminate (annealed at)	d-spacing (Å)	Angular position (2Θ) in degree	Lattice constant (Å)	Cell volume (cm^3)
650 °C	2.4245	37.050	8.0410	519.912
750 °C	2.4259	37.026	8.0460	520.882
850 °C	2.4277	36.998	8.0520	522.049
Zinc aluminate (annealed at)	d-spacing (Å)	Angular position (2Θ) in degree	Lattice constant (Å)	Cell volume (cm^3)
650 °C	2.4244	36.823	8.0890	529.278
750 °C	2.4419	36.775	8.0990	531.244
850 °C	2.4567	36.443	8.1010	531.637

$$a = d\left[\left(h^2 + k^2 + l^2\right)\right]^{1/2} \tag{2}$$

where h, k, and l denote miller indices, d is used for the distance between crystallographic planes, and 'a' is lattice parameter. The structural parameters were evaluated like d-spacing, lattice constant, and cell parameters which are being shown in Table 1a–b.

3.2 Magnetic Measurement and Discussion

Magnetic properties were characterized by using vibrating sample magnetometer (Lake Shore, USA). M-H curves were characterized in the range of magnetic field ±20 kOe. Figure 3a shows M-H curves for the $NiAl_2O_4$ particles at room temperature. It is observed that saturation magnetization (Ms) is not attained even in the high magnetic field of 20 kOe. The same trend is observed for all three samples. The M-H curve declares the magnetization behavior of $NiAl_2O_4$ particles that are paramagnetic at room temperature. From Table 2, it is clear that coercivity and retentivity increase regularly with increase in annealing temperature, while saturation magnetization is approximately steady with slight variation in the values. This is due to crystallite size, broken exchange bond, and the increases in annealing temperature. As the particle size increases, the magnetization increases. Similar behavior was also reported [31].

M-H curve of zinc aluminate for the same three annealing temperatures such as 650, 750, and 850 °C is depicted in Fig. 3b. The magnetic behavior of zinc aluminate samples was investigated by magnetic field between ±20 kOe. M-H curves are showing diamagnetic behavior of zinc aluminate. Coercivity values do not follow a regular pattern, while magnetization values increase smoothly. The coercivity (Hc), magnetization (Ms), and retentivity (Mr) have been enlisted in Table 3. The maximum coercivety was found 909.86 G for nickel aluminates.

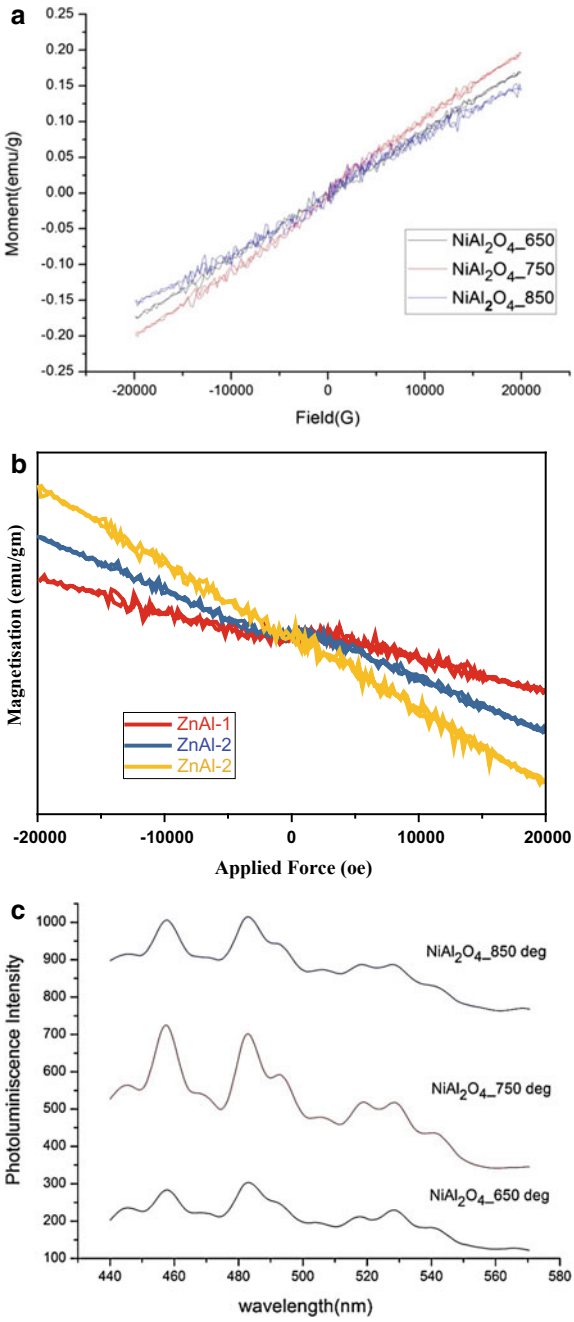

Fig. 3 **a** M-H curve of $NiAl_2O_4$ for three different annealing temperatures. **b** M-H curve of $ZnAl_2O_4$ for three different annealing temperatures. **c** Photoluminescence spectra of $NiAl_2O_4$. **d** Photoluminescence spectra of $ZnAl_2O_4$

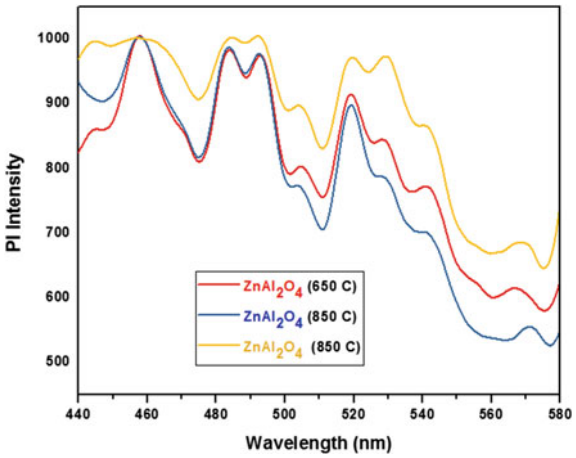

Fig. 3 (continued)

Table 2 Magnetic parameters of nickel aluminate

Magnetic parameters	Nickel aluminate at 650 °C	Nickel aluminate at 750 °C	Nickel aluminate at 850 °C
Coercively (H_c) Oe	104.41G	208G	909.86G
Magnetization (Ms) (emu/gm)	0.17338	0.1984	0.1522
Retentivity (Mr) (emu/gm)	3.3063×10^{-3}	8.396×10^{-4}	6.926×10^{-4}

Table 3 Magnetic parameters of zinc aluminate

Magnetic parameters	Zinc aluminate at 650 °C	Zinc aluminate at 750 °C	Zinc aluminate at 850 °C
Coercivity (H_c) Oe	109.76G	29.759G	264.08G
Magnetization (Ms) (emu/gm)	0.0972	0.1620	0.2473
Retentivity (Mr) (emu/gm)	2.7146×10^{-3}	3.9744×10^{-3}	4.0578×10^{-4}

3.3 Photoluminescence Measurement

In order to understand the fluorescence mechanism of the prepared $ZnAl_2O_4$ and $NiAl_2O_4$ samples, schematic band diagram best examples the excitation phenomenon as well as emission for the system. PL spectra for $NiAl_2O_4$ and $ZnAl_2O_4$ were excited by 200 nm wavelength resulted in an intense blue emission using Perkin Elmer photoluminescence spectroscopy. In the wavelength window of (420–580) nm, the reflected optical spectrum was obtained for aluminates as shown in Fig. 3c, d. The PL spectrum of the both nickel aluminate and zinc aluminate samples annealed at different temperatures are in visible range. In nickel aluminate

sample annealed at 750 °C, PL peaks intensity are sharp and higher compared to sample annealed at 850 and 650 °C. On the other hand, in nickel aluminates, all the emissions peaks are in visible range.

But the peak intensities are not prominent. This may be due to size dependent properties. Further study needed the actual mechanism of this phenomenon. This is our future plan. Most interesting things is that emission are in visible range, which may be useful for various applications [32, 33]. The emission peaks near 480, 519, and 530 nm (known as red shift) might be due to oxygen vacancies. This is called green emission. It is obvious that PL emission is getting shifted with the change in particle size and shape, which supports the results of XRD data suggesting average crystallize size as 8 nm, 12 nm, and 14 nm, respectively. Such PL emission was also reported [34].

4 Conclusion

The nanosized zinc and nickel aluminate nanoparticles were synthesized using low-cost citrate precursor method. The XRD study confirmed that pure phase nickel and zinc aluminate nanoparticles are formed having space group Fd3m. The PL measure measurement shows that the material shows both blue and green emissions this might be due to the oxygen vacancies and defects created in the nanomaterials. These materials will show good photocatalytic and optoelectronic properties and can be used in varied applications. Similarly, the material shows decrease in saturation magnetization and corresponding increase in coercivity showing the size dependency on magnetic properties.

Acknowledgements The authors would like to extend their sincere appreciation to the Aryabhatta Knowledge University Patna, and Dept. Of Education, Govt. of Bihar for their well established scientific laboratory, as all the characterization were done in their laboratories

References

1. Busca G, Lorenzelli V, Escribano VS, Guidetti R (1991) J Catal 131:167
2. Michel CR, Rivera J, Martinez AH, Aranda MS (2008) J Electrochem Soc 155:263
3. Cavalcante PMT, Dondi M, Guarini G, Raimondo M, Baldi G Dyes Pigments 80(209):226
4. Dhak D, Pramanik P (2006) J Am Ceram Soc 89:1014
5. Tzing WS, Tuan WH (1996) J Mater Sci Lett 15:1395–1396
6. Bouropoulos N, Tsiaoussis I, Poulopoulos P, Roditis P, Baskoutas S (2008) Mater Lett 62:3533–3535
7. Khaledi AG, Afshar S, Jahromi HS (2012) Mater Chem Phys 135:855–862
8. Liang Z, Guang-Fu J, Feng Z, Zi-Zheng G (2011) Chin Phys B 20:047102–047107
9. Sickafus KE, Wills JM, Grimes NW (1999) J Am Ceram Soc 82:3279–3292
10. Salavati-Niasari M, Davar F (2009) Mater Lett 63:441–443
11. Gao X, Li X, Yu W (2005) J Phys Chem B 109:1155–1161

12. Roesky R, Weiguny J, Bestgen H, Dingerdissen U (1999) Appl. Catal A:Gen. 176:213–220
13. Dussault L, Dupin JC, Guimon C, Monthioux M, Latorre N, Ubieto T, Romeo E (2007) J Catal 251:223–232
14. Li W, Li J, Guo J (2003) J Eur Ceram Soc 23:2289–2295
15. Platero EE, Arean CO, Parra JB (1999) Res Chem Intermed 25:187
16. Melo DMA, Cunha JD, Fernandes JDG, Bernardi MI, Melo MAF, Martinelli AE (2003) Mater Res Bull 38:1559–1564
17. Shaheen WM (2002) Thermochim Acta 385:105–116
18. Valenzuela MA, Jacobs JP, Bosch P, Reijne S, Zapata B, Brongersma HH (1997) Appl Catal A: Gen 148:315–324
19. Zawadzki M, Wrzyszcz J (2000) Mater Res Bull 35:109–114
20. Chen Z, Shi E, Zheng Y, Li W, Wu N, Zhong W (2002) Mater Lett 56:601–605
21. Adak AK, Pathak A, Pramanik P (1998) J Mater Sci Lett 17:559–561
22. Phani AR, Passacantando M, Santucci S (2001) Mater Chem Phys 68:66–71
23. Hong W-S, De Jonghe LC, Yang X, Rahaman MN (1995) J Am Ceram Soc 78:3217–3224
24. van der Laag NJ, Snel MD, Magusin PCMM, de With G (2004) J Eur Ceram Soc 24:2417–2424
25. Wei X, Chen D (2006) Mater Lett 60:823–827
26. Duan X, Yuan D, Wang X, Xu H (2005) J. Sol-Gel Sc. & Tech. 35:221–224
27. Kumar RT, Selvam NCS, Ragupathi C, Kennedy LJ, Vijaya JJ (2012) Powd. Tech. 224:147–154
28. Khaledi AG, Afshar S, Jahromi HS (2012) Mat. Chem. & Phy. 135:855–862
29. Bragg WH (1915) Phil Mag 30:305–315
30. Scherrer P (1918) Bestimmung der Grösse und der inneren Struktur von Kolloidteilchen mittels Röntgenstrahlen, Nachrichten von der Gesellschaft der Wissenschaften, Göttingen, pp 98–100
31. Singh RK, Yadav A, Narayan A, Chandra M, Verma RK (2012) J Therm Anal Calorim 107:205–210
32. Raghupathi C, Juditya Vijya J, John Kennedy L (2014) Mat Sci Engg B 184:18–25
33. Jung M, Kim S, Ju S (2011) Opt Mat 33:280–283
34. Suresh K, Sampath CF, James J (1998) of Ameri. Ceram. Soci. 81:649–654